The Astrophysical Journal, 629:108–114, 2005 August 10

OBSERVATIONS OF THE BL LACERTAE OBJECT 3C 66A WITH STACEE

D. A. Bramel,[1] J. Carson,[2] C. E. Covault,[3] P. Fortin,[4] D. M. Gingrich,[5,6] D. S. Hanna,[4] A. Jarvis,[2] J. Kildea,[4] T. Lindner,[4] R. Mukherjee,[1,7] C. Mueller,[4] R. A. Ong,[2] K. Ragan,[4] R. A. Scalzo,[8] D. A. Williams,[9] and J. Zweerink[2]

Received 2005 January 5; accepted 2005 April 24

ABSTRACT

We present the analysis and results of recent high-energy gamma-ray observations of the BL Lac object 3C 66A conducted with the Solar Tower Atmospheric Cerenkov Effect Experiment (STACEE). During the 2003–2004 observing season, STACEE extensively observed 3C 66A as part of a multiwavelength campaign on the source. A total of 33.7 hr of data was taken on the source, plus an equivalent-duration background observation. After cleaning the data set a total of 16.3 hr of live time remained, and a net on-source excess of 1134 events was seen against a background of 231,742 events. At a significance of 2.2 σ this excess is insufficient to claim a detection of 3C 66A but is used to establish flux upper limits for the source.

Subject headings: BL Lacertae objects: individual (3C 66A) — galaxies: active — gamma rays: observations

1. INTRODUCTION

To date, all confirmed extragalactic sources of TeV (10^{12} eV) photons have been low-redshift, high-frequency peaked BL Lac objects (HBLs) (Horan & Weekes 2004). Of all BL Lac objects, it is reasonable that nearby HBLs, with their very energetic synchrotron emission, would be the first to be detected at TeV energies. As the energy thresholds of ground-based gamma-ray telescopes decrease and their sensitivities increase, there is significant potential for growth in the number of very high energy (VHE) gamma-ray sources to include higher redshift objects and low-frequency BL Lac objects (LBLs). The LBL 3C 66A is a likely candidate for detection with future VHE telescopes because it was detected in the 30 MeV–20 GeV energy band by the EGRET gamma-ray satellite instrument on the *Compton Gamma Ray Observatory*, has a higher energy synchrotron peak than most LBLs, and already has an unconfirmed TeV detection. The object 3C 66A also has a higher redshift than any confirmed TeV source. In the context of the possible absorption of gamma rays by intergalactic radiation fields, the greater redshift of the source may indicate that detectors with improved sensitivity to energies at or below 100 GeV, such as the Solar Tower Atmospheric Effect Experiment (STACEE), will be able to confirm its detection.

The LBL 3C 66A was first optically identified by Wills & Wills (1974). It is highly variable in the optical and X-ray bands (Maccagni et al. 1987) and shows significant optical polarization (Takalo et al. 1996). It has been extensively observed in the radio and optical, but the host galaxy surrounding the blazar jet has not been resolved. Observations with the Very Long Baseline Array by Jorstad et al. (2001) show a highly superluminal jet, confirming that beamed emission likely plays a major role in the observed flux. The redshift for the source is widely quoted at 0.444, but the scant data supporting this value are highly uncertain (see § 2).

At MeV–GeV energies, 3C 66A is associated with the EGRET source 3EG J0222+4253 (Hartman et al. 1999). This association is not unique, however, as the error box for 3EG J0222+4253 also covers a nearby pulsar, PSR 0218+42. The EGRET source position is consistent with both 3C 66A and the pulsar, but the significance of the association varies with energy (Kuiper et al. 2000). Position contours derived from low-energy (100–300 MeV) photons favor the pulsar location, while high-energy (>1 GeV) contours exclude the pulsar and correlate well with 3C 66A. From this, it is concluded that the pulsar is the primary source of the softer photons detected by EGRET, and 3C 66A is the source of the harder component of the spectrum. Thus, it can be expected that the 3EG J0222+4253 spectral index (-2.01 ± 0.14) is a lower limit for the 3C 66A spectral index and that 3C 66A should produce more high-energy photons than otherwise would be predicted.

Above the EGRET energy range, 3C 66A observations have been largely unsuccessful. Repeated detections above 900 GeV by the Crimean Astrophysical Observatory's GT-48 imaging atmospheric Cerenkov telescope (Neshpor et al. 1998; Stepanyan et al. 2002) at an average integral flux level of 2.4×10^{-11} cm^{-2} s^{-1} have yet to be confirmed at other observatories. Observations by the Smithsonian Astrophysical Observatory's Whipple 10 m gamma-ray instrument produced a 99.9% integral flux upper limit above 350 GeV of $<1.9 \times 10^{-11}$ cm^{-2} s^{-1} in 1993 (Kerrick et al. 1995) and again of $<0.35 \times 10^{-11}$ cm^{-2} s^{-1} in 1995 (Horan et al. 2004), while observations by the HEGRA telescope array in 1997 (Aharonian et al. 2000) produced a 99% upper limit above 630 GeV of $<1.4 \times 10^{-11}$ cm^{-2} s^{-1}. This uncertainty grants 3C 66A a "C" rating in the TeV source summary of Horan & Weekes (2004), placing it among the most tenuous of TeV sources.

As a potential gamma-ray source, 3C 66A is interesting for what it could reveal about the density of extragalactic background light (EBL). At TeV energies, gamma rays can interact with infrared EBL photons, causing a decrease in the observed

[1] Department of Physics, Columbia University, New York, NY 10027.
[2] Department of Physics and Astronomy, UCLA, Los Angeles, CA 90095.
[3] Department of Physics, Case Western Reserve University, 10900 Euclid Avenue, Cleveland, OH 44106.
[4] Department of Physics, McGill University, 3600 University Street, Montreal, QC H3A 2T8, Canada.
[5] Centre for Subatomic Research, University of Alberta, Edmonton, AB T6G 2N5, Canada.
[6] TRIUMF, Vancouver, BC V6T 2A3, Canada.
[7] Department of Physics and Astronomy, Barnard College, New York, NY 10027.
[8] Current address: Lawrence Berkeley National Laboratory, 1 Cyclotron Road, Berkeley, CA 94720.
[9] Santa Cruz Institute for Particle Physics, University of California, Santa Cruz, 1156 High Street, Santa Cruz, CA 95064.

TeV flux that is related to the column density of the EBL photons (Primack et al. 1999; Malkan & Stecker 2001). A redshift of 0.444 would place 3C 66A further away than any confirmed TeV source to date and would make any observed TeV flux highly sensitive to the effects of EBL absorption. Extrapolation of the 3EG spectrum with no EBL absorption predicts a 100 GeV source flux around 0.2 crab, but actual 3C 66A emission could in fact be higher given the pulsar confusion in the 3EG source.

Modeling of the 3C 66A gamma-ray flux by Costamante & Ghisellini (2002) predicts a moderate flux of $(7.0\text{–}9.6) \times 10^{-11}$ cm^{-2} s^{-1} above 40 GeV, but negligible flux ($<0.14 \times 10^{-11}$ cm^{-2} s^{-1}) above 300 GeV. Without EBL absorption, 3C 66A has the potential to be an easily detected TeV source, and for this reason detections and upper limits of the source are very useful for EBL studies. A low predicted EBL cutoff energy of 100–200 GeV (Primack et al. 1999) puts 3C 66A out of reach for many older Cerenkov detectors, but newer instruments may be able to push below the cutoff energy.

The Solar Tower Atmospheric Cerenkov Effect Experiment (STACEE) is a wavefront-sampling Cerenkov detector sensitive to photons above 100 GeV. No previous observations of 3C 66A have been reported by any instrument with a gamma-ray energy threshold in the 100–300 GeV range. The expected high-energy cutoff for 3C 66A is thus a unique and interesting challenge for lower energy ground-based Cerenkov detectors such as STACEE.

The observations described in this paper were taken as part of a 3C 66A multiwavelength campaign (Boettcher et al. 2004). This campaign took place during the 2003–2004 observing season and included optical monitoring by the Whole Earth Blazar Telescope (WEBT) collaboration, X-ray monitoring by the *Rossi X-Ray Timing Explorer* (*RXTE*), VHE gamma-ray observations by STACEE and VERITAS (Weekes et al. 2002), and long-term radio monitoring. In addition, nine high-spatial-resolution observations using the VLA were carried out during the campaign and throughout 2004 to follow possible structural changes of the source. In this paper we describe only the high-energy gamma-ray observations with STACEE (see also Bramel 2005).

2. THE 3C 66A REDSHIFT

The high redshift associated with 3C 66A is one of the main features that sets it apart from most potential TeV sources. The commonly quoted value of 0.444, we believe, may have caused many in the TeV field to dismiss 3C 66A as an undetectable source due to EBL considerations. As part of our work on this object, we have conducted an extensive literature investigation of the widely quoted redshift value and find that the data that back it up are remarkably uncertain. Although not central to the results published in this paper, it is important that the nature of this redshift value be made known to the blazar community, particularly as 3C 66A may play a significant role in future TeV measurements of EBL absorption.

To date, redshift measurements of 3C 66A have been reported in only two papers. The first, Miller et al. (1978), is most widely credited with the $z = 0.444$ measurement. Unfortunately, the redshift value given in this paper for 3C 66A has been so widely quoted in catalogs and summaries over the intervening years that the qualifications of the original work have been generally disregarded. In the paper, Miller et al. call 3C 66A "one of two [objects] in our study for which we feel we still have not measured a definitive redshift," and of the single emission feature detected on the source, they note that "we are not certain of the reality of the feature." They summarize with the admonition that "the redshift 0.444 cannot be considered reliable, and the object deserve[s] more attention."

The second paper on the topic is that of Kinney et al. (1991), which reports on a reprocessing of *International Ultraviolet Explorer* (*IUE*) data taken in the early 1980s. In this reanalysis it is noted that a "weak feature near 1750 Å could be Lyα emission at the object redshift of 0.444," but Kinney et al. also indicate that Crenshaw et al. (1990) found a detector artifact at the same location. For a point-source spectrum, Crenshaw et al. find that the region around 1750 Å shows an excess of $(2\text{–}3) \times 10^{-15}$ ergs cm^{-2} s^{-1} Å^{-1} that is created by the *IUE* instrument itself. The weak feature mentioned by Kinney et al. is not more than 3×10^{-15} ergs cm^{-2} s^{-1} Å^{-1} above the continuous source background. A close examination of the 3C 66A IUE spectrum in this region reveals a strong resemblance, both in structure and in amplitude, to the *IUE* point-source artifact spectrum. Without reanalysis that explicitly accounts for detector artifacts, the validity of using the *IUE* data to confirm the redshift is questionable.

There are no other detections of emission lines for 3C 66A in the literature, though there have been several attempts (e.g., Wills & Wills 1974, 1976). The data for both the initial detection and later confirmation of the 0.444 redshift are not, in our opinion, sufficient to ensure a reliable result. We find it reasonable to hold the value of 3C 66A's redshift in question, and we encourage further spectroscopic observations of this source.

3. THE STACEE DETECTOR

STACEE (Hanna et al. 2002; Chantell et al. 1998) is operational at the National Solar Thermal Test Facility near Albuquerque, NM. It uses 64 large (37 m^2) heliostat mirrors to focus Cerenkov light from gamma-ray–initiated extensive air showers onto an array of 64 photomultiplier tubes (PMTs), with each heliostat mapped onto a unique PMT. High-speed electronics measure the charges and relative arrival times of the PMT pulses. A multilevel coincidence trigger (Martin & Ragan 2000) is used to select Cerenkov events. In this fashion the detector samples the Cerenkov wavefront at 64 separate locations on the ground, making STACEE a *wavefront-sampling* detector. Other gamma-ray detectors utilizing a similar technique include CELESTE (de Naurois et al. 2002) and Solar Two (Tripathi et al. 2002). The large mirror area obtained with the heliostats allows for the detection of faint Cerenkov light pulses and grants a lower energy threshold than all but the newest imaging Cerenkov telescopes.

STACEE utilizes a two-level trigger to discriminate Cerenkov shower events from randomly coincident night-sky background (NSB) photons. The 64 channel array is broken up into eight clusters, each containing eight PMT channels. The signals from each PMT are sampled by discriminators set at a fixed threshold of approximately 5 photoelectrons. The first-level (L1) trigger requires at least five out of eight channels to have a discriminator hit within a 16 ns window. The second-level (L2) trigger then requires at least five of the eight clusters to trigger within the same 16 ns coincidence window before recording a Cerenkov event. For each Cerenkov trigger, 1 GS s^{-1} flash ADCs (FADCs) are used to digitize the pulse on each channel, preserving all the information contained in the wavefront sample.

STACEE has been fully operational since 2001 and has detected gamma rays from the Crab Nebula (Oser et al. 2001) and Mrk 421 (Boone et al. 2002). It has also collected data on a number of active galactic nuclei (Kildea et al. 2005). A full

description of the STACEE detector can be found in Gingrich et al. (2005).

4. DATA AND ANALYSIS

Observations with STACEE are performed in on-off pairs, whereby a source is observed for 28 minutes followed by a 28 minute observation of an equivalent off-source area of dark sky. Each off-source observation covers the same azimuth and elevation range as the corresponding on-source observation. By using this technique, each instant of on-source data has exactly one equivalent instant of off-source data, and comparisons between halves of a pair are inherently corrected for observation angle–dependent systematics. The difference between the on- and off-source shower detection rates is attributed to photons coming from the direction of the source. Since the off-source observations are required for background estimation, an on-off pair is considered to be the base unit of a STACEE observation. Background for STACEE consists almost entirely of hadron-initiated air showers.

During the 2003–2004 observation season, 85 on-off pairs were taken on 3C 66A. These pairs totaled 33.7 hr of on-source live time prior to the data-cleaning process, plus an equal amount of off-source live time. A series of data-cleaning criteria, or "cuts," were applied to remove known hardware malfunctions, including removal of sections in which one or more heliostats were not operational, the high-voltage system had tripped off, or parts of the data acquisition system were inoperative. After the application of hardware cuts, a total of 29.3 hr on source remained.

4.1. *Data-Quality Cuts*

A set of cuts was applied to the data that were focused on removing apparent or potential problems caused by unfavorable weather conditions. A cut was made to remove all data that could potentially be contaminated by frost buildup on the heliostat mirrors, as even a small amount of condensation on the optics causes significant degradation in the detector performance. The frost potential was determined by looking at the records of the atmospheric frost index (defined to be the difference between the atmospheric temperature and the dew point) during data taking. Any data taken while the frost index was below $5^{\circ}.5$ C were discarded.

A second data-quality cut was made to remove data biased by clouds or changing atmospheric opacity. The L1 cluster rates are driven primarily by accidental coincidences stemming from NSB photons and thus are sensitive to changes in background light levels. At the STACEE site, light pollution is high enough that any increase in sky opacity due to clouds, haze, or other atmospheric phenomena causes a distinct increase in the NSB rate. Accordingly, the L1 trigger rate provides a measure of the stability of the observing conditions. Stable nights produce steady L1 rates, while unstable nights show significant L1 rate fluctuations.

Since the NSB noise is elevation dependent, no attempt was made to constrain L1 rates to an absolute range. Instead, we used the cuts to constrain the correlation between on- and off-source L1 rates. The data were divided into 30 s intervals, and the average L1 rates on- and off-source were calculated for each interval. A correlation statistic $\theta_{\rm L1}$ was defined for each interval based on the L1 rates,

$$\theta_{\rm L1} = \ln\left(\frac{\rm L1_{on}}{\rm L1_{off}}\right), \tag{1}$$

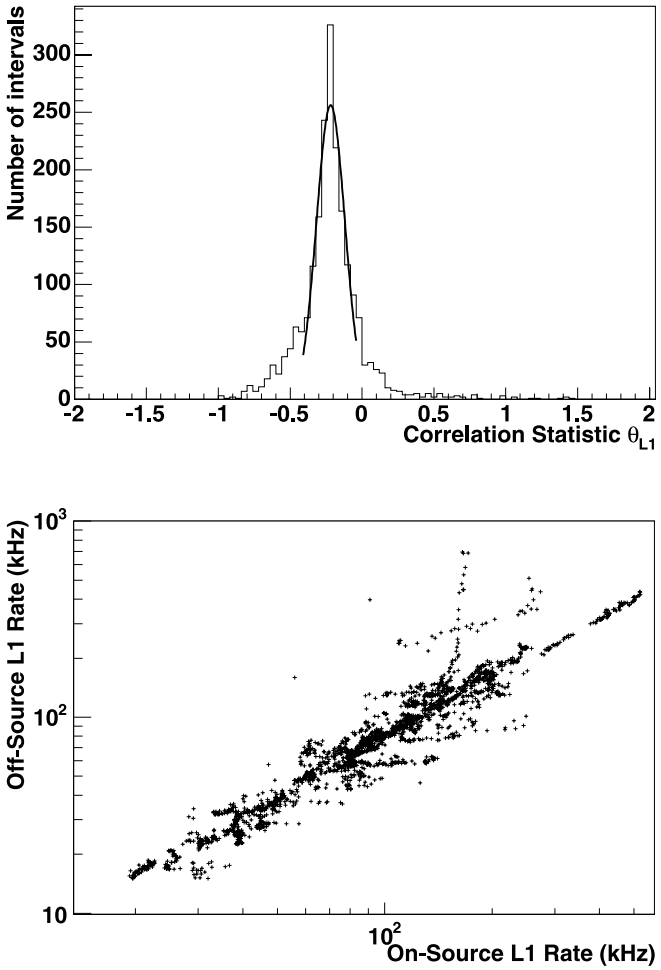

FIG. 1.—Distribution of the L1 rate correlation statistic for a single cluster over the entire 3C 66A data set. The top panel shows a histogram of the correlation statistic. Normal variation in the L1 trigger rates are shown by the central Gaussian peak of the distribution, while unstable weather conditions cause the non-Gaussian wings. The bottom panel shows a scatter plot of the L1 trigger rates for on- and off-source data. Changes in the ratio of the trigger rates due to clouds and haze can be seen in the feathery fringes in the scatter plot.

giving a characteristic measure of the correlation between the on- and off-source L1 rates. Histograms of this statistic for each cluster were then compiled over the entire data set (see Fig. 1). For data that are unaffected by sky opacity changes, this distribution of $\theta_{\rm L1}$ for each cluster should be Gaussian, indicating only random variations of the correlation statistic. In practice, a Gaussian peak with extended tails is obtained, indicating nonrandom variation caused by changing cloud cover. By performing a Gaussian fit to the peaks of the distributions and discarding data in which the correlation statistic of any cluster lies more than 2 σ from the mean value for that cluster, sections of data that have been contaminated by clouds and haze were removed.

A second, similar type of quality cut is made with the occupancy of each channel. The occupancy of a channel is defined as the average fraction of triggers in which the channel has a discriminator hit. With stable observing and hardware conditions, the on- and off-source occupancies should be highly correlated. We define an occupancy correlation statistic for a single channel similar to that of equation (1),

$$\theta_{\rm occ} = \ln\left(\frac{\rm occ_{on}}{\rm occ_{off}}\right), \tag{2}$$

and cut on the distribution of this quantity in the same way as with the L1 statistic. Because of the larger number of channels that are being constrained, there is a higher likelihood of a large fluctuation in good-quality data than with the L1 cuts. To avoid eliminating these data, we remove only data with three or more channels having occupancy statistic values more than 3 σ from the mean value for that channel or with any one channel having an occupancy statistic value more than 5 σ from the mean value for that channel.

After application of all data-quality selection cuts, a total of 16.8 hr of on-source data remained.

4.2. *Padding*

The measured background rate can be systematically biased by variations in the brightness of the sky in the field of view of the detector, often referred to as the *field brightness*. When an observing field is bright, the increased NSB photon count results in increased levels of event promotions (dim Cerenkov showers that trigger simply because they are boosted above threshold by random NSB photons). Thus, we expect bright fields to yield higher trigger rates than dark fields.

The field brightness can change between on- and off-source observations as a result of weather instability, but even very stable nights show a field brightness difference due to the different stars in each field. The brightness difference due to field stars is often rather small: the number and magnitude of stars falling inside the $\sim 1^\circ$ STACEE field of view tend to be roughly constant, and the promotion contributions from each field cancel each other out. However, for certain sources an individual bright star in one field upsets the balance (see, e.g., Boone et al. 2002); the result is a highly distorted background measurement that if followed blindly, results in a spurious source excess or deficit.

To counter the effects of field brightness differences, a technique called "software padding" is employed. Software padding effectively increases the light level of the darker half of the pair by adding a sample trace containing only NSB background to each event's FADC trace. Once the light level is increased, a software trigger criterion is applied to both halves of each pair. This padding technique, described in detail in Scalzo et al. (2004), has been shown to effectively remove the effects of field brightness differences in STACEE data. Data used in the 3C 66A analysis presented here were padded using the waveform library technique of Scalzo et al. (2004). Cuts to remove sections of the data for which the padding algorithm was unable to execute were also applied, leaving a total net live time of 16.3 hr on source.

5. RESULTS

After all time cuts and padding, we are left with 1134 excess on-source events over a net observation time of 16.3 hr. The excess events are against an off-source background of 231,742 events, yielding an on-source excess significance of 2.2 σ using the method of Li & Ma (1983). This excess significance is not sufficient to claim a detection of the source. There were no significant transient events in the data, as shown by the histogram of significances for each of the 85 pairs in Figure 2.

6. DETECTOR SIMULATIONS

In order to best understand the results of the observations of 3C 66A, simulations of the STACEE detector were carried out to closely mimic the 3C 66A data set. Using the CORSIKA air-shower simulation package (Heck et al. 1998), sets of showers were simulated with gamma-ray, proton, and helium primaries. These were generated over a range of energies and source hour angle (H) positions. Cerenkov photons from each shower were passed through a custom-made optics simulation package and converted into photoelectrons by simulated PMTs. These resultant photoelectrons were run through a custom-made electronics simulation to determine which showers would have triggered the array.

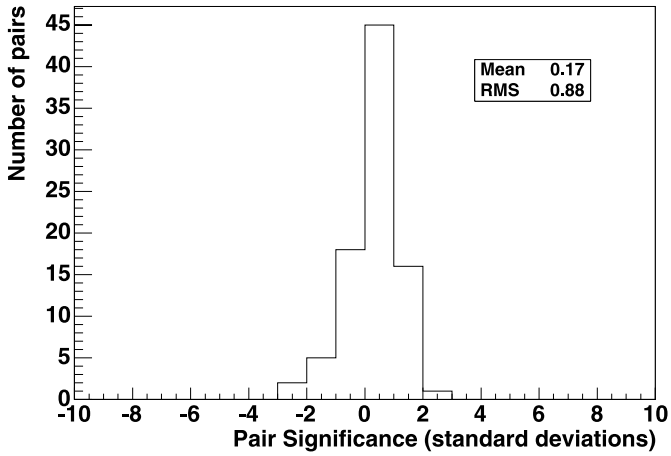

FIG. 2.—Histogram of the significance value, in σ, for each on-off pair in the post-cut data taken by STACEE on the source 3C 66A. The fact that there are no on-off pairs having significance values far from zero indicates that no significant transient events were seen.

Parameters for the custom simulation packages were specified to match operational detector parameters as closely as possible. All fixed detector parameters, such as coincidence conditions and electronics configurations, were set in simulation to be identical to the detector as it was during data taking. Variable parameters that affect detector performance, such as PMT currents, were set to the average values taken from data with an hour angle similar to that of the simulated showers. In this way, each simulated shower was processed with simulated parameters as close as possible to the data it was intended to simulate. The simulation is able to reproduce several diagnostic quantities seen in the data, including L1 rates and cosmic-ray trigger rate as a function of source hour angle.

Once the simulated showers were processed through the simulation pipeline, analysis was carried out in the same manner as for real data.

6.1. *Effective Area*

To determine the sensitivity of the STACEE detector we have to determine its effective area, the sensitive area presented to incoming gamma rays. The effective area of the array was determined for each shower type by scattering simulated showers across the detector, then multiplying the triggered fraction by the total scattering area. Scattering areas were circular in the plane normal to the arrival direction of the primary particle, with radii sufficiently large that triggers near the edge of the area were negligible.

Effective areas were calculated as a function of energy E at several hour angles H for each shower primary type. We interpolated between the discrete effective area points and then weighted the effective area by the source observation time to obtain a net effective area as a function of energy:

$$A_{\rm eff}(E) = \frac{\int A_{\rm eff}(H,\ E) X(H)\, dH}{\int X(H)\, dH}, \qquad (3)$$

where the exposure $X(H)$ was taken from the post-cut live time in the real data set. This net effective area, computed separately

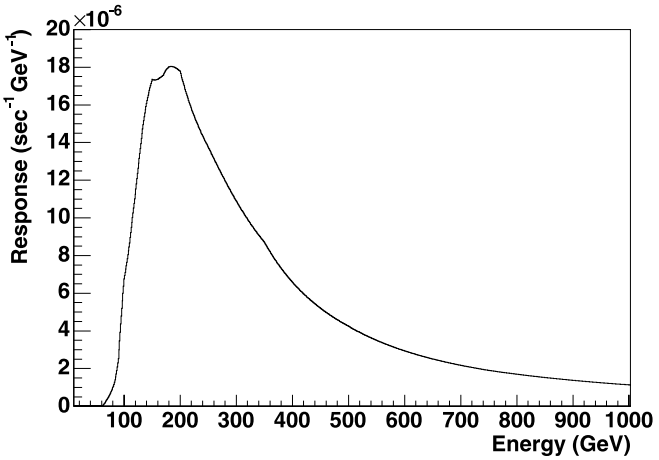

FIG. 3.—Post-cut energy response curve of the STACEE detector for an example power-law photon spectrum with a differential spectral index of −2.5. The peak of the response curve defines the energy threshold E_{th} of the detector, though STACEE is sensitive to photons below E_{th}.

for each primary particle type, is the effective area of STACEE relevant for the 3C 66A data set.

6.2. *Energy Threshold and Flux Upper Limit*

Using the simulated effective area, we calculated detector energy thresholds and source flux upper limits. Following convention, the energy threshold E_{th} is defined as the peak of the response curve generated when the effective area of the detector is convolved with a source spectrum, as shown in Figure 3. The lack of any known spectral properties for 3C 66A in the STACEE energy range adds a degree of uncertainty to the estimation of the energy threshold and flux upper limits. These estimates depend heavily on the assumed shape of the source spectrum. At EGRET energies, the spectrum of 3C 66A is known to be quite hard, fitting a power-law photon differential index no softer than -2.01 ± 0.14. At higher energies, above 20 GeV, the spectrum no doubt falls off more steeply due to intrinsic softening and EBL absorption, but neither of these effects is well constrained. The amount of EBL absorption is particularly uncertain because the redshift value of the source is, as argued above, very unreliable.

We present in Table 1 the energy thresholds and flux upper limits derived from the observations, for a variety of power-law and EBL-absorbed power-law spectra.

TABLE 1
INTEGRAL FLUX UPPER LIMITS

	$\Gamma = \infty$ [a]		$\Gamma = 200$ [a]	
SPECTRAL INDEX	E_{thresh} [b]	99% Confidence Limit[c]	E_{thresh} [b]	99% Confidence Limit[c]
−2.0	200	<1.0	150	<1.9
−2.5	184	<1.2	150	<1.9
−3.0	150	<1.7	142	<2.1
−3.5	147	<1.8	137	<2.3

NOTE.—The 99% confidence limits on the 3C 66A photon flux are derived in this work, assuming an EBL-absorbed power-law spectrum with photon index α and exponential EBL cutoff energy Γ.

[a] Exponential EBL cutoff energy, in units of GeV.

[b] STACEE energy threshold, in units of GeV.

[c] Integral photon flux limit at the energy threshold, in units of 10^{-10} cm^{-2} s^{-1}.

7. SUMMARY AND DISCUSSION

The STACEE experiment observed the BL Lac object 3C 66A for a total of 33.7 hr in the fall of 2003. After all cuts and padding, 16.3 hr of data yielded an on-source excess with a significance of 2.2 σ, consistent with no detected flux. Flux upper limits derived from simulated effective areas are given in Table 1.

Figure 4 shows the full spectral energy distribution (SED) for 3C 66A, made using noncontemporaneous data. Radio–X-ray data have been compiled from the literature and are plotted with 1 σ error bars. Various EGRET detections are shown as open symbols. These include the data of Kuiper et al. (2000), who estimated and subtracted the contribution from the nearby pulsar PSR 0218+42; note that the pulsar-subtracted measurement suggests that the high-energy peak continues to rise steeply into the STACEE energy band. The STACEE limits (*plus signs*) assume an unabsorbed spectrum with the four spectral indices listed in Table 1. They are at a lower energy threshold and higher flux than the TeV limits from the Whipple telescope (Horan et al. 2004) and HEGRA telescope array (Aharonian et al. 2004). A homogeneous, one-zone, synchrotron self-Compton model from Costamante & Ghisellini (2002) is also shown. All of the gamma-ray observations to date, including the STACEE flux limits, are consistent with this model.

In conjunction with simultaneous data at other wavelengths, the STACEE limits presented in Table 1 have the potential to constrain models of the source emission mechanism. However, very little physical modeling of 3C 66A has been published in the literature. Modeling of high-energy gamma-ray emission from BL Lac objects is very complex and depends extensively on simultaneous constraints from lower energy emission. The 2003–2004 multiwavelength campaign, of which the STACEE observations are a part, will produce the first simultaneous set of broadband spectral data on 3C 66A from optical to gamma-ray energies.

Broadband modeling has been successful when applied to simultaneous multiwavelength observations of sources similar to 3C 66A, such as W Comae and BL Lacertae. All three of these BL Lac objects share the similarity that their synchrotron emission is dominant at X-ray energies. According to the *ROSAT*

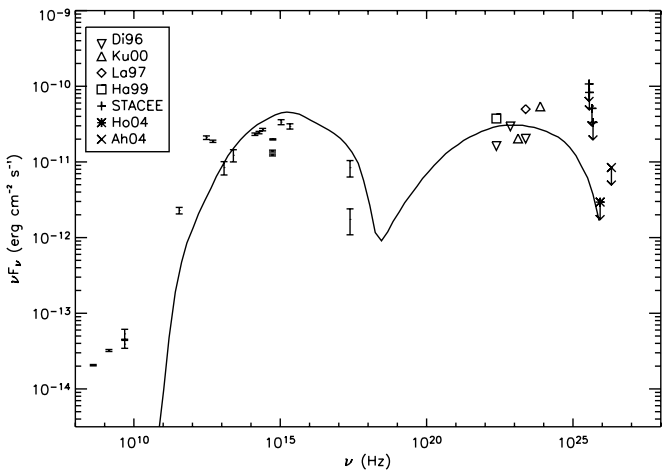

FIG. 4.—Broadband SED for 3C 66A. Radio–gamma-ray measurements have been compiled from the literature. The EGRET detections are plotted as open symbols (Di96: Dingus et al. 1996; Ha99: Hartman et al. 1999; La97: Lamb & Macomb 1997; Ku00: Kuiper et al. 2000). The STACEE flux limits are shown as plus signs. The TeV limits from Whipple and HEGRA are shown as asterisks and crosses, respectively (Ho04: Horan et al. 2004; Ah04: Aharonian et al. 2004).

all-sky survey data, the X-ray spectrum of 3C 66A is soft (spectral index of 1.6; Fossati et al. 1998), indicating that the synchrotron component of 3C 66A extends to the X-ray regime. The *ROSAT* measurement of a soft spectrum for 3C 66A is supported by more recent observations by *XMM-Newton* (Croston et al. 2003) and by *BeppoSAX* (Perri et al. 2003). Higher energy synchrotron emission by these LBLs indicates that they lie closer to the HBL end of the BL Lac spectrum than most LBLs and thus are more likely to have significant TeV emission.

In the past, W Comae and BL Lacertae have been the subject of extensive multiwavelength campaigns. These data have been interpreted using the fully time-dependent leptonic jet simulation code of Böttcher & Chiang (2002) as well as hadronic synchrotron-proton blazar (SPB) models (Muecke et al. 2003). In the case of W Comae, time-dependent modeling of the X-ray variability of the source was found to yield quite different model predictions of the GeV-TeV flux for hadronic or leptonic models (Böttcher et al. 2002). W Comae has thus proved to be a promising target for VHE gamma-ray and coordinated broadband observations, as it may serve to distinguish between leptonic and hadronic jet models for blazars. STACEE flux limits on the >100 GeV emission from W Comae begin to constrain hadronic emission models (Scalzo et al. 2004). Similarly, BL Lacertae was also the subject of an extensive multiwavelength monitoring campaign in 2000, and the data were modeled using leptonic and hadronic jet models to fit the observed broadband spectra and spectral variability patterns (Böttcher & Reimer 2004). Such multiwavelength modeling studies with blazars tell us about cooling timescales, magnetic fields, and Doppler factors associated with blazar jets. Hadronic models for blazar jets predict significantly greater TeV flux than leptonic models, and these differences can be tested by future TeV observations of BL Lac by VERITAS or MAGIC (Moralejo et al. 2004).

Although such modeling is outside the scope of this work, studies are in progress to understand data from the recent 3C 66A multiwavelength campaign using the fully time-dependent leptonic jet simulation code of Böttcher & Chiang (2002) and to use the data from radio through X-ray energies to make predictions about high-energy emission (Böttcher et al. 2005). The implications of the STACEE upper limits on 3C 66A could then be evaluated in the context of the properties of the relativistic jet in 3C 66A, testing leptonic and hadronic models for this source. Model-dependent flux predictions at VERITAS energies can also be made, given a specific model and the STACEE flux upper limits.

Perri et al. (2003) argue that the multiwavelength spectrum and modeling studies of 3C 66A could be applied toward resolving the controversy regarding the identification of 3C 66A/PSR 0218+4232 with the EGRET source. With the pulsar accounting for a majority of the low-energy EGRET photons, the SED of 3C 66A in the EGRET energy range must be steeply rising. Perri et al. (2003) point out that it is difficult to fit the 3C 66A SED from Kuiper et al. (2000) to a log-parabolic approximation of the synchrotron self-Compton (SSC) peak. A simple, smooth model of the SSC peak favors a 3C 66A spectrum that includes the photons attributed to the pulsar by Kuiper et al. (2000). Simultaneous modeling of the broadband 3C 66A spectrum with data at X-ray and TeV energies would be able to help resolve the issue by showing whether or not an additional component is able to fit the Kuiper et al. (2000) spectrum.

Detection of >100 GeV photons from 3C 66A would be a very interesting result for gamma-ray astronomy. Currently, all blazars detected by TeV experiments have been HBL objects; 3C 66A is an LBL object, with a synchrotron peak at lower energies than HBL objects. Confirmation of >100 GeV photons from this source would open the door on a new class of objects for TeV astronomy. In addition, if the redshift of 0.444 is correct, such a confirmation would make 3C 66A the most distant known TeV source. This would make it a very interesting source for constraining EBL spectral models.

It is our hope that the results presented here will motivate further study of this source with a more sensitive detector. The possibility that there may be detectable flux at energies near 100 GeV makes 3C 66A an interesting target for the new generation of imaging Cerenkov telescopes such as VERITAS and MAGIC. Together with GLAST (Thompson et al. 2004) and *AGILE* (Pittori et al. 2004) at lower energies, observations of this source will provide a comprehensive data set at sub-TeV gamma-ray energies that will be important for modeling studies.

We are grateful to the staff at the National Solar Thermal Test Facility, who continue to support our science with enthusiasm and professionalism. This work was supported in part by the National Science Foundation, the Natural Sciences and Engineering Research Council of Canada (NSERC), Fonds Québécois de la Recherche sur la Nature et les Technologies (FQRNT), the Research Corporation, and the University of California at Los Angeles.

REFERENCES

Aharonian, F. A., et al. 2000, A&A, 353, 847
———. 2004, A&A, 421, 529
Boettcher, M., et al. (WEBT Collaboration). 2004, HEAD, 8, 04.10
Boone, L. M., et al. 2002, ApJ, 579, L5
Böttcher, M., & Chiang, J. 2002, ApJ, 581, 127
Böttcher, M., Mukherjee, R., & Reimer, A. 2002, ApJ, 581, 143
Böttcher, M., & Reimer, A. 2004, ApJ, 609, 576
Böttcher, M., et al. 2005, ApJ, in press
Bramel, D. 2005, Ph.D. thesis, Columbia Univ.
Chantell, M. C., et al. 1998, Nucl. Instrum. Methods, A408, 468
Costamante, L., & Ghisellini, G. 2002, A&A, 384, 56
Crenshaw, D. M., Bruegman, O. W., & Norman, D. J. 1990, PASP, 102, 463
Croston, J. H., Hardcastle, M. J., Birkinshaw, M., & Worrall, D. M. 2003, MNRAS, 346, 1041
de Naurois, M., et al. 2002, ApJ, 566, 343
Dingus, B. L., et al. 1996, ApJ, 467, 589
Fossati, G., Maraschi, L., Celotti, A., Comastri, A., & Ghisellini, G. 1998, MNRAS, 299, 433
Gingrich, D. M., et al. 2005, in Trans. IEEE Nucl. Sci., in press
Hanna, D. S., et al. 2002, Nucl. Instrum. Methods, A491, 126
Hartman, R. C., et al. 1999, ApJS, 123, 79
Heck, D., Knapp, J., Capdevielle, J., Schatz, G., & Thouw, T. 1998, FZKA Rep. 6019
Horan, D., & Weekes, T. C. 2004, NewA Rev., 48, 527
Horan, D., et al. 2004, ApJ, 603, 51
Jorstad, S. G., Marscher, A. P., Mattox, J. R., Wehrle, A. E., Bloom, S. D., & Yurchenko, A. V. 2001, ApJS, 134, 181
Kerrick, A. D., et al. 1995, ApJ, 452, 588
Kildea, J., et al. 2005, in AIP Conf. Proc. 745, High Energy Gamma-Ray Astronomy, ed. Felix A. Aharonian, H. J. Völk, & D. Horns (New York: AIP), 481
Kinney, A. L., Bohlin, R. C., Blades, J. C., & York, D. G. 1991, ApJS, 75, 645
Kuiper, L., Hermsen, W., Verbunt, F., Thompson, D. J., Stairs, I. H., Lyne, A. G., Strickman, M. S., & Cusumano, G. 2000, A&A, 359, 615
Lamb, R. C., & Macomb, D. J. 1997, ApJ, 488, 872
Li, T.-P., & Ma, Y.-Q. 1983, ApJ, 272, 317
Maccagni, D., Garilli, B., Schild, R., & Tarenghi, M. 1987, A&A, 178, 21
Malkan, M. A., & Stecker, F. W. 2001, ApJ, 555, 641
Martin, J. P., & Ragan, K. 2000, Proc. IEEE, 12, 141
Miller, J. S., French, H. B., & Hawley, S. A. 1978, in Pittsburgh Conference on BL Lac Objects (A79-30026 11-90; Pittsburgh: Univ. Pittsburgh, Dept. Phys. Astron.), 176

Moralejo, A., et al. (MAGIC Collaboration). 2004, Mem. Soc. Astron. Italiana, 75, 232
Muecke, A., Protheroe, R. J., Engel, R., Rachen, J. P., & Stanev, T. 2003, Astropart. Phys. 18, 593
Neshpor, Y. I., Stepanyan, A. A., Kalekin, O. P., Fomin, V. P., Chalenko, N. N., & Shitov, V. G. 1998, Astron. Lett., 24, 134
Oser, S., et al. 2001, ApJ, 547, 949
Perri, M., et al. 2003, A&A, 407, 453
Pittori, C., et al. (AGILE Team). 2004, HEAD, 8, 16.05
Primack, J. R., Bullock, J. S., Somerville, R. S., & MacMinn, D. 1999, Astropart. Phys., 11, 93
Scalzo, R. A., et al. 2004, ApJ, 607, 778
Stepanyan, A. A., Neshpor, Y. I., Andreeva, N. A., Kalekin, O. R., Zhogolev, N. A., Fomin, V. P., & Shitov, V. G. 2002, Astron. Rep., 46, 634
Takalo, L. O., et al. 1996, A&AS, 120, 313
Thompson, D. J., et al. (GLAST Large Area Telescope Collaboration). 2004, HEAD, 8, 30.06
Tripathi, S. M., et al. 2002, BAAS, 34, 676
Weekes, T. C., et al. 2002, Astropart. Phys., 17, 221
Wills, B. J., & Wills, D. 1974, ApJ, 190, L97
Wills, D., & Wills, B. J. 1976, ApJS, 31, 143